

Cheap but accurate calculation of chemical reaction rate constants from ab initio data, via system-specific, black-box force fields

Julien Steffen, and Bernd Hartke

Citation: [The Journal of Chemical Physics](#) **147**, 161701 (2017);

View online: <https://doi.org/10.1063/1.4979712>

View Table of Contents: <http://aip.scitation.org/toc/jcp/147/16>

Published by the [American Institute of Physics](#)

Articles you may be interested in

[A general intermolecular force field based on tight-binding quantum chemical calculations](#)
The Journal of Chemical Physics **147**, 161708 (2017); 10.1063/1.4991798

[Intermolecular interactions in the condensed phase: Evaluation of semi-empirical quantum mechanical methods](#)
The Journal of Chemical Physics **147**, 161704 (2017); 10.1063/1.4985605

[Perspective: Dissipative particle dynamics](#)
The Journal of Chemical Physics **146**, 150901 (2017); 10.1063/1.4979514

[Perspective: Found in translation: Quantum chemical tools for grasping non-covalent interactions](#)
The Journal of Chemical Physics **146**, 120901 (2017); 10.1063/1.4978951

[Interpolation of intermolecular potentials using Gaussian processes](#)
The Journal of Chemical Physics **147**, 161706 (2017); 10.1063/1.4986489

[Extension of the D3 dispersion coefficient model](#)
The Journal of Chemical Physics **147**, 034112 (2017); 10.1063/1.4993215



Cheap but accurate calculation of chemical reaction rate constants from *ab initio* data, via system-specific, black-box force fields

Julien Steffen and Bernd Hartke^{a)}

Institut für Physikalische Chemie, Christian-Albrechts-Universität, Olshausenstraße 40, D-24098 Kiel, Germany

(Received 1 February 2017; accepted 10 March 2017; published online 14 April 2017)

Building on the recently published quantum-mechanically derived force field (QMDFF) and its empirical valence bond extension, EVB-QMDFF, it is now possible to generate a reliable potential energy surface for any given elementary reaction step in an essentially black box manner. This requires a limited and pre-defined set of reference data near the reaction path and generates an accurate approximation of the reference potential energy surface, on and off the reaction path. This intermediate representation can be used to generate reaction rate data, with far better accuracy and reliability than with traditional approaches based on transition state theory (TST) or variational extensions thereof (VTST), even if those include sophisticated tunneling corrections. However, the additional expense at the reference level remains very modest. We demonstrate all this for three arbitrarily chosen example reactions. Published by AIP Publishing. [<http://dx.doi.org/10.1063/1.4979712>]

I. INTRODUCTION

Simulation of chemical reactions on macroscopic time scales can be achieved by ignoring almost all molecular dynamics details and coarse-graining each elementary reaction step to a probability or rate $k(T)$ as a function of temperature, to convert reactants to products in a single, coarse-grained step. With established procedures like kinetic Monte Carlo (KMC; see Refs. 1 and 2 for an introduction and a review, respectively), it is then possible to simulate complex chemical reaction networks over long time scales, for example, in heterogeneous catalysis.³ Clearly, this radical coarse-graining needs $k(T)$ data as input, for all possible elementary reaction steps. Hence, ways to produce such $k(T)$ data are needed, which ideally work in black-box fashion and deliver these data with small computational effort but in good quality.

Reaction rate constants $k(T)$ can be calculated exactly or approximately, with a broad range of methods based on classical, semiclassical, or quantum mechanics.^{4–7} There are tricks to avoid full reactive scattering calculations and to circumvent the rare-event problem, both in classical-mechanical dynamics^{8–10} and in quantum mechanics.^{11–16} Nevertheless, practically useful accuracy has to be bought by an accurate representation of the potential energy surface (PES) at least in a region around the transition state or by employing on-the-fly *ab initio* dynamics, both of which are computationally highly expensive.

For example, $k(T)$ calculation via transition-state theory (TST)^{17,18} has big advantages: It avoids the rare-event problem by replacing dynamics with statistical thermodynamics and only needs PES data (energies and frequencies) at two points, at the reactant minimum and at the transition state (TS). Hence it is computationally cheap, even if done directly at some *ab initio* quantum-chemistry level. However, it also

makes several approximations: (1) separability of the reaction coordinate from all others, (2) no recrossing of the dividing surface between reactants and products, (3) dividing surface tied to the TS, and (4) harmonic approximation in the calculation of partition functions. These approximations do lead to significant errors for many reactions.^{17,18} They also pose fundamental challenges: For example, in classical mechanics, TST rates converge to the exact classical-mechanical rate in the limit of very small excess energies, but exactly in this limit tunneling is most important (albeit absent in classical mechanics).

Variational TST (VTST)¹⁹ alleviates problem (3) to some extent, by optimizing the position of the dividing surface. Various types of tunneling corrections²⁰ can further improve the results. Finally, the full $k(T)$ calculation can be divided into two parts: (a) TST or VTST to get from the reactants to the dividing surface and (b) full dynamics starting from the dividing surface to produce a “transmission coefficient.”^{8–10} This division eliminates problem (2). All this, however, incurs additional computational expense: further PES information has to be calculated, up to re-introducing full dynamics on the PES.

This re-increase of computational expense could be minimized to almost zero if a simple but accurate force-field representation of the *ab initio* PES were available. This idea has been tested before, for example, in Ref. 20. The present work re-exploits this idea, using as force field the empirical valence bond combination of two quantum-mechanically derived force fields (EVB-QMDFFs) presented in recent work.^{21,22} EVB-QMDFF is advantageous because it can be constructed in black-box fashion from a small set of well-defined reference data for essentially arbitrary elementary reaction steps, but still delivers impressive accuracy.

In the presence of a good force field, $k(T)$ can be calculated with advanced methods that need many PES points. In the present work, we employ ring-polymer molecular dynamics (RPMD)^{23–30} for this purpose. RPMD delivers quantum

^{a)}Author to whom correspondence should be addressed. Electronic mail: hartke@pctc.uni-kiel.de

corrections without *ad hoc* recipes and allows the user to choose freely from a broad spectrum of trade-offs between low expense (close to classical mechanics) and high accuracy (close to quantum mechanics).

RPMD has been shown³¹ to provide good agreement in $k(T)$ -calculations with full quantum-mechanical wavepacket dynamics results, even for difficult systems like FH + Cl which shows strong tunneling and frequent transition-state recrossings due to the chattering motion of the transferring hydrogen atom.

As a side effect, the present work significantly extends our previous EVB-QMDFF work²² in two respects: First, several EVB coupling models established in the literature are tested for EVB-QMDFF and are found to improve the overall PES quality in difficult cases where a simple coupling with one energy-dependent Gaussian is too inflexible. Second, the present work answers a question not fully covered before, namely, how good is the EVB-QMDFF-PES in many or all degrees of freedom perpendicular to the reaction path. Our results show that EVB-QMDFF indeed is sufficiently accurate for the purpose of $k(T)$ calculations. Hence, this strategy (combination of EVB-QMDFF with RPMD) offers a low-expense approach to a black-box-like mass production of $k(T)$ data with useful accuracy.

II. METHODOLOGY AND IMPLEMENTATION

Full details of the EVB-QMDFF construction and three application problems of differing difficulty have been presented in the original EVB-QMDFF paper²² and will not be repeated here. For completeness, we only mention some of the key points.

As shown by Grimme,²¹ the isolated potential energy wells of reactants and products, respectively, can be accurately represented by QMDFF, for essentially any reasonable chemical system. These QMDFFs are created using a fixed and very small set of reference data (energy, frequencies, CMS charges,³² and Wiberg-Mayer bond orders^{33,34}) for the respective minimum structures. Full details of the QMDFF function and parametrization can be found in the original publication.²¹ Briefly, QMDFF is designed in analogy to traditional non-reactive force fields. The force constants are found by minimizing the deviations between Hessians of reference and QMDFF using the Levenberg-Marquardt algorithm. Due to scans of all torsional angles and simple extended Hückel calculations on them, a QMDFF is able to reproduce other torsional minima of the bonded structure, in addition to the single reference minimum. Last but not least, QMDFF is fully anharmonic and can describe dissociations of all bonds in the system, with reasonable accuracy. However, one QMDFF can only describe the molecular configuration that is given by the input bond pattern and bond orders. In particular, although bonds can dissociate in QMDFF, no reactions can be described in which new bonds are formed.

In a recent paper by one of the present authors,²² it was shown that a simple coupling of two QMDFFs (for reactants and products) leads to an extended model (EVB-QMDFF) that allows formation of new bonds, with excellent accuracy. From various coupling methods advocated in the literature,³⁵

the empirical valence bond (EVB) idea by Warshel^{36,37} was chosen.

In EVB-theory, two diabatic potential functions $F_1(\mathbf{q})$ and $F_2(\mathbf{q})$ are coupled by an arbitrary coupling term $C(\mathbf{q})$. This can be done mathematically by diagonalizing the respective EVB matrix (Eq. (1)) for any given point \mathbf{q} in coordinate space,

$$\begin{pmatrix} F_1(\mathbf{q}) & C(\mathbf{q}) \\ C(\mathbf{q}) & F_2(\mathbf{q}) \end{pmatrix}. \quad (1)$$

For a 2×2 -system, this diagonalization can be done analytically. The resulting lower eigenvalue represents the energy of the coupled system at geometry \mathbf{q} ,

$$V(\mathbf{q}) = \frac{1}{2}(F_1(\mathbf{q}) + F_2(\mathbf{q})) \pm \sqrt{\left[\frac{1}{2}(F_1(\mathbf{q}) - F_2(\mathbf{q}))\right]^2 + C^2(\mathbf{q})}. \quad (2)$$

As shown in the original EVB-QMDFF paper,²² this yields a good reproduction of 1D reaction paths, even for the rather simple coupling function of one Gaussian which simply depends on the energy difference between both diabatic potential functions,

$$C(\mathbf{q}) = a \exp(-b[F_1(\mathbf{q}) - F_2(\mathbf{q})]^2). \quad (3)$$

The two variable parameters a and b can be optimized with respect to the best possible reproduction of the energies along the reaction path. This surprisingly simple EVB approach is well known from the literature^{38–40} and works fine in many investigated example reactions. However, there is a considerable amount of reactions for which it results in larger errors along the reaction path and especially in the transition region. In the worst cases, artificial minima are created there. Possible reasons for this behavior are sharp or highly unsymmetric shapes of transition regions which handicap the performance of one single Gaussian coupling function. In other words, more sophisticated coupling functions with higher adaptability to the needed changes of coupling along the reaction path are needed here.

We have investigated several possibilities for new coupling functions in EVB-QMDFF. One possible solution is the linear combination of more (e.g., N) Gaussians at different locations near the transition state,

$$C(\mathbf{q}) = \sum_{i=1}^N a_i \exp(-b_i[(F_1(\mathbf{q}) - F_2(\mathbf{q})) - c_i]^2). \quad (4)$$

The additional parameters c_i for each Gaussian provide a shift of the center away from the transition state. To optimize this coupling term for a distinct reaction, $3N$ parameters need to be optimized, in contrast to the two parameters before. This can be done with local optimization, for example, the Levenberg-Marquardt algorithm.^{41,42} To improve the ability of finding the global minimum in this multivariate search, we have enhanced the local optimization with multistart local search using randomized starting points in an interval defined by the user for each of the variables. In the case of more than one Gaussian with different centers, problems might occur if two Gaussians come close to each other. If that happens, numerical instabilities might occur. To avoid that, a restraint was added to the optimization which defines a minimal difference of two c_i values.

Another possibility is to change the variable which determines the coupling strength. Instead of using the energy difference $F_1(\mathbf{q}) - F_2(\mathbf{q})$, one could also use the distance of the actual molecular structure \mathbf{q} from the transition state \mathbf{q}_{TS} , in terms of internal coordinates,

$$C(\mathbf{q}) = \sum_{i=1}^N a_i \exp(-b_i[\mathbf{q} - \mathbf{q}_{TS}]^2). \quad (5)$$

This type of coupling shall be termed ΔQ -coupling, in contrast to the above coupling depending on the energy difference (ΔE). For ΔQ -coupling, one can also combine several Gaussians at different positions, analogous to Eq. (4). To perform the ΔQ -coupling, the geometry of the transition state for the reaction needs to be optimized using the reference *ab initio* method.

Some of the investigated reactions were problematic for ΔE -coupling but could be represented well with ΔQ -coupling. However, a subset of the investigated reactions caused problems with both coupling types.

In the literature, further methods have been proposed for constructing an appropriate EVB coupling term, using additional input from the reference PES. The Minchino-Voth,⁴³ Chang-Miller,^{44,45} and the related DG-EVB methods^{46–48} are based on Taylor expansions of $C(\mathbf{q})$ around a number of points on the PES. The multi-configuration molecular mechanics (MCMM), now called multi-configuration Shepard interpolation (MCSI) method,^{20,49,50} is based on Shepard interpolation between those reference points.

We have decided to use the DG-EVB ansatz which seemed suitable for re-implementation. Other implementations were done in a Mathematica Toolkit^{47,51} and as a part of the Amber program suite^{48,52} by the original authors.

The foundation of the method is to solve Eq. (2) for $C(\mathbf{q})$ which results in

$$C^2(\mathbf{q}) = [F_1(\mathbf{q}) - V(\mathbf{q})] [F_2(\mathbf{q}) - V(\mathbf{q})]. \quad (6)$$

Hence the reference energy $V(\mathbf{q})$ and energies of both QMDFFs ($F_1(\mathbf{q})$, $F_2(\mathbf{q})$) are needed to calculate the desired coupling at a point \mathbf{q} . If one takes the derivative of Eq. (6) with respect to the coordinates, the gradient and Hessian matrix of the coupling can be obtained and expressed in terms of gradients and Hessians from reference and QMDFFs on a number of chosen points. The QMDFF gradient is calculated analytically and Hessians are done numerically.

Based on the Chang-Miller coupling term, the following expression can be derived for the DG-EVB coupling term.⁴⁶

$$C^2(\mathbf{q}) = \sum_K^M \sum_{i \geq j \geq 0}^{3N} b_{ijK} g(\mathbf{q}, \mathbf{q}_K, i, j, \alpha_K). \quad (7)$$

For each location K on the PES, s-, p-, and d-functions (corresponding to $g(\mathbf{q}, \mathbf{q}_K, 0, 0, \alpha_K)$, $g(\mathbf{q}, \mathbf{q}_K, i, 0, \alpha_K)$, and $g(\mathbf{q}, \mathbf{q}_K, i, j, \alpha_K)$, respectively, cf. Eq. (8)) are introduced into the coupling term, analogous to basis functions in quantum chemistry. The indices i and j assign the i 'th or j 'th value of the coordinate vectors \mathbf{q} or \mathbf{q}_K , respectively,

$$\begin{aligned} g(\mathbf{q}, \mathbf{q}_K, 0, 0, \alpha) &= \exp\left[-\frac{1}{2}\alpha|\mathbf{q} - \mathbf{q}_K|^2\right], \\ g(\mathbf{q}, \mathbf{q}_K, i, 0, \alpha) &= (\mathbf{q} - \mathbf{q}_K)_i \exp\left[-\frac{1}{2}\alpha|\mathbf{q} - \mathbf{q}_K|^2\right], \\ g(\mathbf{q}, \mathbf{q}_K, i, j, \alpha) &= (\mathbf{q} - \mathbf{q}_K)_i (\mathbf{q} - \mathbf{q}_K)_j \exp\left[-\frac{1}{2}\alpha|\mathbf{q} - \mathbf{q}_K|^2\right]. \end{aligned} \quad (8)$$

Additionally, first and second derivatives for all the Gaussians are calculated (numerically) and are stored into the matrix \mathbf{D} .

The coefficients b_{ijK} are optimized to achieve exact reproduction of the needed couplings and their derivatives (stored in vector \mathbf{f}). $C(\mathbf{q})$, $dC(\mathbf{q})/d\mathbf{q}$, and $d^2C(\mathbf{q})/d\mathbf{q}^2$ are expressed as linear combinations of the Gaussians and their derivatives from the matrix \mathbf{D} . This results in a system of linear equations that can be solved to obtain the needed coefficient vector \mathbf{b} ,

$$\mathbf{Db} = \mathbf{f}. \quad (9)$$

If this system is solved, all b_{ijK} values are determined. However, the exponential prefactors α_K are still undetermined by the above procedure. They describe the width of the summarized Gaussians at each reference point and hence the width of the overall coupling, which obviously influences the deviation between EVB-QMDFF and the reference PES. We have chosen to optimize the exponential prefactors α_K by simple multi-start local search combined with Levenberg-Marquardt,^{41,42} to reproduce the energies on the reaction path as well as possible (as for the ΔE and ΔQ terms stated above). In each optimization cycle, Eq. (9) needs to be solved again with the actual α_K values for the Gaussian functions. To the best of our knowledge, this is the first time that α_K are optimized systematically in a DG-EVB implementation.

For practical reasons, it is useful to reduce the set of internal coordinates \mathbf{q} to a manually chosen subset Γ that contains the coordinates changing significantly during the reaction.

The given gradients and Hessians of QMDFFs and the reference method can be transformed from the given Cartesian coordinates into this chosen set of Γ coupling coordinates with the usual coordinate transformations.⁵³

All described EVB coupling terms were implemented into our Fortran90 program named EVB-QMDFF. A flowchart of this EVB-QMDFF program is shown in Figure 1. The generation of QMDFFs and the calculation of their energies and analytical gradients were done using the original QMDFF Fortran77 program written by Grimme.²¹

Our EVB-QMDFF program calls the Grimme QMDFF program whenever energies or gradients are needed. The DG-EVB method was designed such that an arbitrary set of internal coordinates Γ chosen by the user can be read in. Additionally it allows us to vary the given input data for the reference points in DG-EVB. The simplest mode is only to use energies, followed by the usage of energies and gradients, and finally the full coupling term with energies, gradients, and Hessians. In case of larger systems, it might be more useful to skip Hessians in order to reduce costs for reference as well as EVB-QMDFF calculations. More reference points may be chosen instead in a compensatory manner.

To run dynamics and to calculate rate constants, a program from the literature, RPMDrate by Suleimanov,^{54,55} was used. This program manages the calculation of RPMD rate

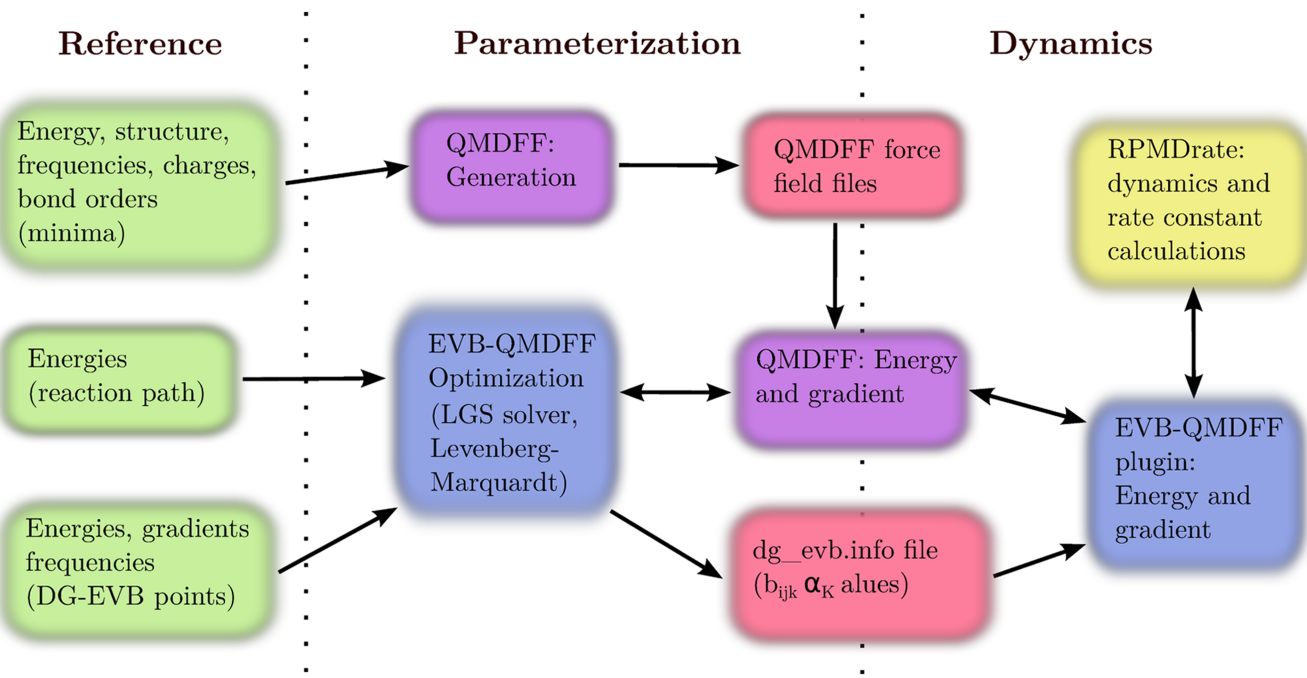


FIG. 1. A flowchart of the EVB-QMDFF program implemented in this work, for the case of a DG-EVB-QMDFF calculation. The needed reference data are marked green, the QMDFF program by Grimme is marked violet, our own EVB-QMDFF code is blue, written intermediate input files are red, and the RPMDRate program by Suleimanov is yellow. Parametrization and dynamics calculations are performed as separate jobs.

coefficients based on umbrella samplings on several beads and following recrossing calculations. It calls the gradient by a Python-Fortran interface whenever it is needed. A modified version of the EVB-QMDFF program was taken as plugin to deliver the energy and gradient to RPMDRate.

In case of more than one equivalent reaction path (high symmetry of reactants), RPMDRate allows the inclusion of more than one equivalent transition state. However, this means that more than one parametrized reaction path is sampled. This would need an EVB with more than two diabatic states in the case of the radicalic hydrogen abstractions. To avoid this problem, we used only the parametrized transition state and corrected the reaction rates by the symmetry number (σ_{Ei}) of the educts,

$$k(T)_{\text{total}} = k(T)_{\text{RPMDRate}} \cdot \sigma_{E1} \cdot \sigma_{E2}. \quad (10)$$

III. COMPUTATIONAL DETAILS

All quantum chemical calculations for the three presented example reactions were performed using the Gaussian09⁵⁶ and ORCA⁵⁷ software packages. Since CM5 charges and Wiberg-Mayer bond orders are only available with ORCA, these data needed to be calculated using ORCA in each example. On the other hand, intrinsic reaction coordinate (IRC) scans⁵⁸ for reaction paths cannot be done with it, so Gaussian needs to be used for this part.

For the nucleophilic substitution $\text{Cl}^- + \text{CH}_3\text{Br}$, all reference data were calculated with density functional theory (DFT) using ORCA. The optimization of the transition state as well as C–Cl and C–Br distance scans towards both minima was done using the PBE0 functional⁵⁹ with the D3 dispersions correction,⁶⁰ the def2-QZVPP(-g, -f) basis set,^{61,62} a dense

“grid5” integration grid, and a “tight” SCF threshold. Both minima were optimized and CM5 charges and Wiberg-Mayer bond orders were found with the same methodology.

The two radicalic hydrogen abstraction reactions $\text{OH} + \text{NH}_3$ and $\text{CH}_2\text{O} + \text{CH}_3$ were treated with MP2 and the cc-pVTZ basis set.⁶³ Transition state optimization as well as the following IRC calculations and optimizations of the minima were done using the Gaussian program suite. Gradients and frequencies on six respectively seven chosen points on the reaction path were also calculated with Gaussian. For the optimized structures of the minima, CM5 charges and Wiberg-Mayer bond orders are obtained from ORCA calculations using the same methods stated above.

The QMDFFs of the minima for all reactions were optimized using the original program package by Grimme. To correct the small deviations in the reproduction of the reference minimum energies introduced by the force constant optimizations, the QMDFF energies were shifted manually to an exact reproduction of the energy at the reference structures. (These corrections are included in the energy plots (Figures 3 and 4).)

EVB coupling terms were optimized with the EVB-QMDFF program package mentioned in Sec. II. The $\text{Cl}^- + \text{CH}_3\text{Br}$ reaction was parametrized using the ΔE coupling term from Eq. (3). This parametrization was also used in the first EVB-QMDFF paper by one of the current authors.²² The optimization, done by hand in Ref. 22, was now done with the multi-start local search Levenberg-Marquardt algorithm, utilizing the energies on the reaction path as equally weighted reference data.

For the radical hydrogen abstractions, the ΔE term gave bad results (Figure 3); therefore, the DG-EVB coupling method was used here. Four coupling coordinates were chosen for the $\text{OH} + \text{NH}_3$ reaction and two for the $\text{CH}_2\text{O} + \text{CH}_3$

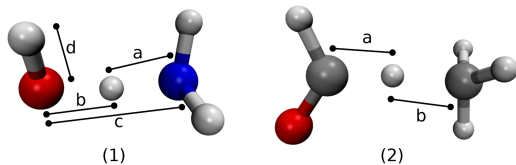


FIG. 2. Chosen set Γ of internal coordinates used for DG-EVB coupling in the $\text{OH} + \text{NH}_3$ (left) and the $\text{CH}_2\text{O} + \text{CH}_3$ (right) reactions. The structures shown are the transition states for both reactions, respectively. It can be seen that for the first reaction, four distances were used, whereas two distances were chosen in the second.

reaction, depicted in Figure 2. How this choice was made is explained in the first section of the [supplementary material](#) to the present publication. Briefly, for the present purposes, four different sets of coordinates that are changing significantly during the reaction were preselected for each of the two reactions, and the performance of EVB-QMDFF along the reaction path for different numbers of reference points was investigated for these sets. All investigated coordinates performed reasonably; the set that gave the best results was chosen. More systematical and automatized approaches are to be implemented in the future, for example, similar approaches to those used in wave packet dynamics.^{64,65}

For both hydrogen abstraction reactions energies, gradients and Hessians with *ab initio* reference information on seven points along the reaction path are included. One of these seven points is the transition state and three others are located on both sides of this point. Further explanations can be found in the [supplementary material](#). On first tests referring to calculations of rate constants with the other DG-EVB modes (energies, and energies + gradients), it became apparent that only the full description with energies, gradients, and Hessians leads to rate constants with an accuracy as shown below. The other modes resulted in rate constants differing more strongly from the experimental values or had problems in the umbrella sampling stage, presumably because of sharp PES changes near the reaction path.

As reference data for the α_K optimization, the energies of the reaction path were used, similar to the ΔE coupling in the first example.

For comparison, $k(T)$ values were also calculated with TST and VTST using the POLYRATE program⁶⁶ by Truhlar and co-workers. Its purpose is the calculation of classical and quantum-corrected rate constants from *ab initio* or first principles reference data at the educts/products, the transition state, and (optionally) the reaction path. The POLYRATE reaction rates are compared with the RPMDrate reaction rates below. To guarantee a fair contest between both programs, the same reference data were used, except for the optimized structures of the single educts/products and their energies and frequencies needed for POLYRATE.

Only for the $\text{Cl}^- + \text{CH}_3\text{Br}$ reaction, additional data on the path were produced for POLYRATE, because this information is needed for calculations of rate constants beyond the simple TST formula.

Energies, gradients, and frequencies for six additional points on the optimized path of $\text{Cl}^- + \text{CH}_3\text{Br}$ were calculated for this purpose, using the same methodology mentioned above (in addition to the TS frequencies which are not used in the

case of ΔE coupling). The POLYRATE program allows the import of precalculated quantum chemistry data via the “unit 40 protocol.” A script written for this purpose was used to translate our quantum chemical results into the POLYRATE format.

Another possibility to investigate the quality of the EVB-QMDFF force field is to calculate TST and canonical variational theory/small curvature tunneling (CVT/SCT) $k(T)$ values with POLYRATE using the EVB-QMDFF results as input data. These $k(T)$ values can be compared with the constants calculated based on the *ab initio* reference. For that purpose, the needed EVB-QMDFF data of minima and points on the reaction path were calculated and included into the POLYRATE “unit 40” file. For the single educts and products, the energies of the *ab initio* reference were taken instead of their EVB-QMDFF counterparts because the latter cannot represent energies for parts of the system. EVB-QMDFF gradients and Hessians can be calculated also for parts of the system, if one considers only the entries that belong to the atoms of the actual educt/product.

For the $\text{OH} + \text{NH}_3$ reaction, Hessian matrices of all points were included into the file, but for the $\text{Cl}^- + \text{CH}_3\text{Br}$ and the $\text{CH}_2\text{O} + \text{CH}_3$ reactions, the normal mode frequencies were included instead. The reason is that the EVB-QMDFF frequencies at the transition state for these reactions contained one or two small imaginary frequencies, respectively, which caused problems when used in POLYRATE unchanged.

TST and CVT rates were then calculated as well as CVT/SCT rates including tunneling corrections for all the example reactions. The chosen reaction temperatures were the same as for RPMDrate (cf. Table 2 in the [supplementary material](#)).

Finally, RPMD reaction rates using the parametrized EVB-QMDFF surfaces were calculated. This was done with the RPMDrate program^{54,55} which calls our code for the calculation of gradients (Figure 1). The settings for the RPMDrate calculations are presented in the [supplementary material](#). Most of those settings were taken from publications that presented other applications of RPMDrate.^{67–69} To demonstrate the ability of the EVB-QMDFF surfaces to produce reliable reaction rates at a broader temperature range, four different temperatures were used for each example. The temperatures were selected following the available experimental data. The number of beads was raised in situations where larger quantum effects could be expected. These cases are low temperatures and light atoms to be transferred (as it is the case in both radical hydrogen abstractions). More systematical investigations of some settings (the number of beads, the size of time step, and the number of biased sampling trajectories) are done also in the [supplementary material](#).

In both radical hydrogen abstraction reactions, a substantially larger umbrella force constant needed to be used. Due to the sharp transition region of the reactions, a weaker force constant leads to an insufficient sampling of the transition region which caused rather bad results or errors.

At the end of this section, we summarize the general procedure of setting up an EVB-QMDFF. For both reactant and product QMDFFs, the reference data prescribed by the QMDFF construction consist of the energy, partial charges,

bond orders, and frequencies, at the quantum-chemical minimum. For the EVB coupling term between the minima, the amount of reference data needed depends on the used coupling term. In the simplest case of a ΔE coupling, only energies along a reaction path are needed. In the most common case of DG-EVB coupling, energies, gradients, and Hessians of the transition state and ideally some points on both sides of it are needed, in addition to reaction path energies. Additionally, a suitable set of internal coordinates for the coupling should be chosen, containing the most active coordinates. Details for how to perform these selections, and on convergence with respect to the amount of these additional data, are provided in the [supplementary material](#).

For the chosen example reactions, the following reference data items were included: $\text{Cl}^- + \text{CH}_3\text{Br}$: 35 energies (two for QMDFF minima and 33 as reference for the optimization of the ΔE coupling term along the path), two Hessians as QMDFF reference at the chosen minima. $\text{OH} + \text{NH}_3$: 90 energies (two for QMDFF minima, 7 for DG-EVB points which are the TS and three points on both sides, chosen from the reaction path and roughly equally spaced, and 81 energies along the reaction path), 7 gradients for the DG-EVB points, and 9 Hessians (two for the QMDFF minima and 7 for the DG-EVB points). $\text{CH}_2\text{O} + \text{CH}_3$: 96 energies (two for QMDFF minima, 7 for DG-EVB points chosen as in the second reaction, and 87 for the energies on the path), 7 gradients for the DG-EVB points, and 9 Hessians for DG-EVB points and QMDFF minima.

The numbers of these additional single-point energies on the reaction path are fairly large, simply because these data were already available from the optimized IRC. Similarly, in most real-life application cases, such a collection of dozens of single points on the IRC will be available, too, due to the need to verify that the transition state indeed links the reactant and product minima. Nevertheless, in the [supplementary material](#), we show that also much smaller numbers (around 10) of such additional single-point energies give results of almost equal quality.

These steps of choosing and calculating reference data, followed by the force field setup and optimization, can be automatized. Hence it becomes a routine task to produce a reaction-specific force field from scratch, for any reaction of interest. This reaction-specific force field is much more

accurate for this reaction than any general force field could ever be.

IV. RESULTS AND DISCUSSION

A method used for the calculation of rate constants should at least be able to reproduce the energies along the reaction path as well as possible. Additionally, the coupling terms are optimized to reproduce the path energies so that the remaining errors indicate how good the optimization was.

To figure out the ability and the problems of the simple ΔE coupling, its performance for the $\text{Cl}^- + \text{CH}_3\text{Br}$ and the $\text{OH} + \text{NH}_3$ reactions is shown in Figure 3.

The reaction path energies for the $\text{Cl}^- + \text{CH}_3\text{Br}$ reaction are reproduced well and only small deviations in line with chemical accuracy are visible. As expected, the coupling is only relevant in the region between the minima, whereas in the extrapolated regions beyond the minima EVB-QMDFF and QMDFF energies coincide.

A different picture emerges for the reaction path energies of the $\text{OH} + \text{NH}_3$ reaction. Apparently, the coupling term is not able to satisfactorily reproduce the reference. An artificial minimum is located near the transition state. Additionally, energies in the extrapolated regions deviate substantially from the QMDFF energies, which indicates that the coupling is not restricted to the transition state region as it should be.

A possible reason for this bad behavior is the sharp kink of the path near the transition state. One single Gaussian has not a suitable shape to reproduce the needed coupling strength behavior. A simplified illustration of this fact is given by the path energy profile itself (although it is not identical to the coupling): For the $\text{Cl}^- + \text{CH}_3\text{Br}$ reaction, this profile near the TS already has a shape reminiscent of a Gaussian function. This is not true for the $\text{OH} + \text{NH}_3$ reaction; there the transition region approximately has the shape of a Slater function, although upon magnification there is no actual cusp present (Fig. 4).

In Figure 4, reference and DG-EVB-QMDFF energies are plotted for the $\text{OH} + \text{NH}_3$ and the $\text{CH}_2\text{O} + \text{CH}_3$ reactions. In both cases, the DG-EVB terms provide a nearly exact reproduction of the reaction path. Additionally, the coupling is only noticeable in the region around the transition state and the

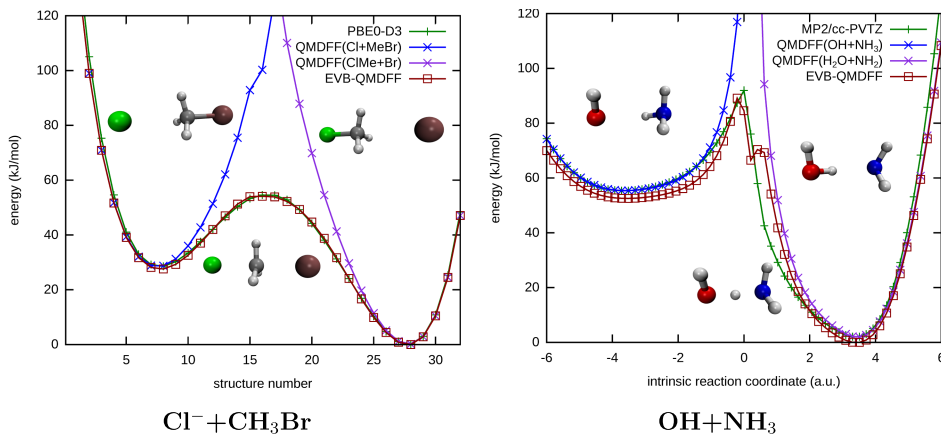


FIG. 3. Energy profiles along the reaction path, for the $\text{Cl}^- + \text{CH}_3\text{Br}^-$ and the $\text{OH} + \text{NH}_3^-$ reaction. Besides the reference energy, energies for both QMDFFs and for the EVB-QMDFF energy are plotted. The simple ΔE coupling term of Eq. (3) was used and optimized for both reactions. While this term achieves a good approximation of the reference in the first example, large deviations occur in the second. The three insets in each picture show molecular structures at the two minima and at the transition state.

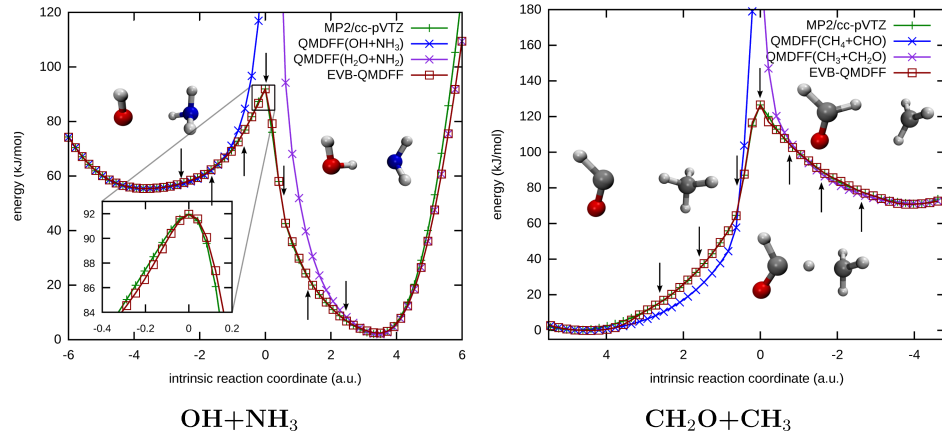


FIG. 4. Energy profiles along the reaction path, for the $\text{OH} + \text{NH}_3$ and the $\text{CH}_2\text{O} + \text{CH}_3$ reaction. Both EVB couplings are parametrized using the DG-EVB coupling model with the set of coordinates shown in Figure 2. In the first case, energies and gradients were used as reference, and in the second case, energies, gradients, and Hessians. The locations of the structures where additional reference data for the DG-EVB were calculated are indicated by black arrows. For the sake of descriptiveness, only each second energy is plotted. To show that the barriers are quite sharp but nevertheless have no discontinuous shape, a zoom onto the transition region is shown for the $\text{OH} + \text{NH}_3$ reaction. The two/three insets in each picture show molecular structures at the two minima and at the transition state.

EVB-QMDFF energies coincide with the QMDFF energies in the extrapolated regions beyond the minima.

However it might be possible that this good agreement disappears in other regions of the many-dimensional potential energy surface, maybe even in the immediate vicinity of the one-dimensional reaction path. For the ΔE coupling, it was already shown that EVB-QMDFF is able to describe the PES beyond the reaction path (cf. supplementary material of Ref. 22).

In the case of DG-EVB, simple Taylor series arguments support the expectation that the gradient (and Hessian) information collected in the DG-EVB coupling parameters should provide a reliable behavior also in regions off the reaction path (but not too far away from it). It is cumbersome and insufficient

to show that this expectation is correct by providing further energy profiles along other degrees of freedom, simply because there are so many of them, even for these small systems. In the supplementary material of the first EVB-QMDFF publication,²² two-dimensional cuts along the two involved bond lengths of the $\text{Cl}^- + \text{CH}_3\text{Br}$ reaction show that EVB-QMDFF indeed approximates the quantum-chemistry PES very well, within this subspace. However, this still is just one particulate view of the PES, out of very many.

Instead of doing more one- or two-dimensional scans, we have calculated reaction rates for all three reactions, one with the simple ΔE coupling term and the other two with DG-EVB including energies, gradients, and Hessians as reference data. During the rate constant calculations with

TABLE I. The calculated rate constants for all three example reactions, in comparison with experimental data (in $\text{cm}^3 \text{molecule}^{-1} \text{s}^{-1}$).

T (K)	TST _{ref.} ^a	TST _{EQ} ^b	CVT	CVT/SCT _{ref.}	CVT/SCT _{EQ}	RPMD	Expt.
$\text{Cl}^- + \text{CH}_3\text{Br} \longrightarrow \text{CH}_3\text{Cl} + \text{Br}^-$							
207	7.60(-06) ^c	5.92(-05)	1.03(-07)	9.90(-08)	1.42(-05)	3.11(-10)	3.10(-11) ^d
300	9.95(-08)	3.65(-07)	2.02(-09)	1.98(-09)	1.69(-07)	8.12(-11)	2.40(-11)
538	2.17(-09)	3.25(-09)	6.68(-11)	6.59(-11)	3.15(-09)	4.07(-11)	1.40(-11)
564	1.79(-09)	2.51(-09)	5.63(-11)	5.56(-11)	6.40(-10)	3.87(-11)	1.40(-11)
$\text{OH} + \text{NH}_3 \longrightarrow \text{H}_2\text{O} + \text{NH}_2$							
300	8.45(-17)	1.96(-17)	2.73(-18)	2.47(-17)	5.26(-17)	8.49(-13)	1.98(-13) ^e
400	1.38(-15)	4.63(-15)	5.20(-17)	1.90(-16)	3.06(-16)	1.11(-12)	4.09(-13)
500	8.12(-15)	3.45(-15)	3.36(-16)	7.95(-16)	1.08(-15)	1.73(-12)	6.93(-13)
600	2.84(-14)	1.43(-14)	1.26(-15)	2.33(-15)	2.82(-15)	2.67(-12)	1.05(-12)
$\text{CH}_2\text{O} + \text{CH}_3 \longrightarrow \text{CHO} + \text{CH}_4$							
700	7.00(-17)	1.57(-17)	2.36(-18)	1.69(-17)	2.03(-17)	4.67(-15)	3.33(-15) ^f
800	2.93(-16)	3.93(-17)	1.03(-17)	5.21(-17)	4.19(-17)	1.21(-14)	8.23(-15)
900	9.34(-16)	8.22(-17)	3.40(-17)	1.32(-16)	7.62(-17)	2.92(-14)	1.84(-14)
1000	2.45(-15)	1.51(-16)	9.17(-17)	2.88(-16)	1.26(-16)	5.28(-14)	3.80(-14)

^aThe subscript ref. means that the POLYRATE unit40 protocol with QM reference data was used.

^bThe subscript EQ means that the POLYRATE unit40 protocol with EVB-QMDFF reference data was used.

^cThe notation 1.52(-05) is an abbreviation for $1.52 \cdot 10^{-5}$.

^dExperimental results from Ref. 70.

^eTaken from the Arrhenius expression of Ref. 71.

^fTaken from the modified Arrhenius expression of Ref. 72.

RPMDrate, large areas of the energetically accessible regions around the reaction path are sampled in all degrees of freedom, so good reaction rates (similar to experimental results) should indicate a good behavior of the EVB-QMDFF surfaces beyond the reaction path. The results are shown and compared with experimental data and TST/CVT rates in Table I. The TST, CVT, and CVT/TST rates are calculated using the quantum-chemical reference (subscript ref). As an intermediate test of how well EVB-QMDFF approximates the reference PES, TST and CVT/SCT rates are also calculated using EVB-QMDFF as reference data (subscript EQ).

The reference as well as the different calculated rate constants are also plotted in terms of a classical Arrhenius plot in Fig. 5.

For the $\text{Cl}^- + \text{CH}_3\text{Br}$ reaction, the RPMDrate reaction rates are slightly too high but still within the same order of magnitude as the experimental data. For the simple coupling term and the DFT reference, this is a satisfying result.

The TST_{ref} and CVT reaction rates show a better performance for higher temperatures than for lower ones. CVT and CVT/SCT_{ref} rates are of the same order of magnitude as the experimental rates only for 538 and 564 K. Deviations much larger than one order of magnitude can be seen for lower temperatures and especially for the TST method. The TST_{EQ} rate constants based on EVB-QMDFF data are within the same order of magnitude as the TST_{ref} values, meanwhile CVT/SCT_{EQ} and CVT/SCT_{ref} deviate one to three orders of magnitude. A possible explanation for these deviations is that the ΔE

coupling term introduces small errors along the reaction path which have greater influence on the CVT/SCT results. In line with this observation are the slightly larger deviations between RPMDrate and experiment in comparison with the other two reactions.

In case of the $\text{OH} + \text{NH}_3$ reaction, much better results are achieved. Experimental and RPMDrate reaction rates deviate only by a factor of two to three, with the calculated rates being slightly too high again. Tunneling-corrected CVT shows roughly the correct temperature dependence; however, the absolute values of the TST_{ref} and CVT/SCT_{ref} rate constants are shifted by three orders of magnitude away from the experimental values. The values based on EVB-QMDFF data (TST_{EQ} and CVT/SCT_{EQ}) are very similar to the values based on MP2 reference data (TST_{ref} and CVT/SCT_{ref}) which shows that the EVB-QMDFF fitting does not introduce PES artifacts. It does, however, make approaches like RPMDrate possible that extensively sample the PES and avoid most approximations. In contrast, TST and CVT/SCT rate constants are based on calculations that use only a very restricted PES sampling (to remain affordable on an *ab initio* level) and more serious approximations, which understandably leads to larger errors.

The $\text{CH}_2\text{O} + \text{CH}_3$ reaction show very good agreements between the reference and the RPMDrate results. They deviate by less than a factor of two from each other, which is the best result of this publication. CVT/SCT shows a similar behavior like in the $\text{OH} + \text{NH}_3$ reaction: Whereas the temperature dependence is reproduced roughly, a shift of approximately two orders of magnitude away from the experimental

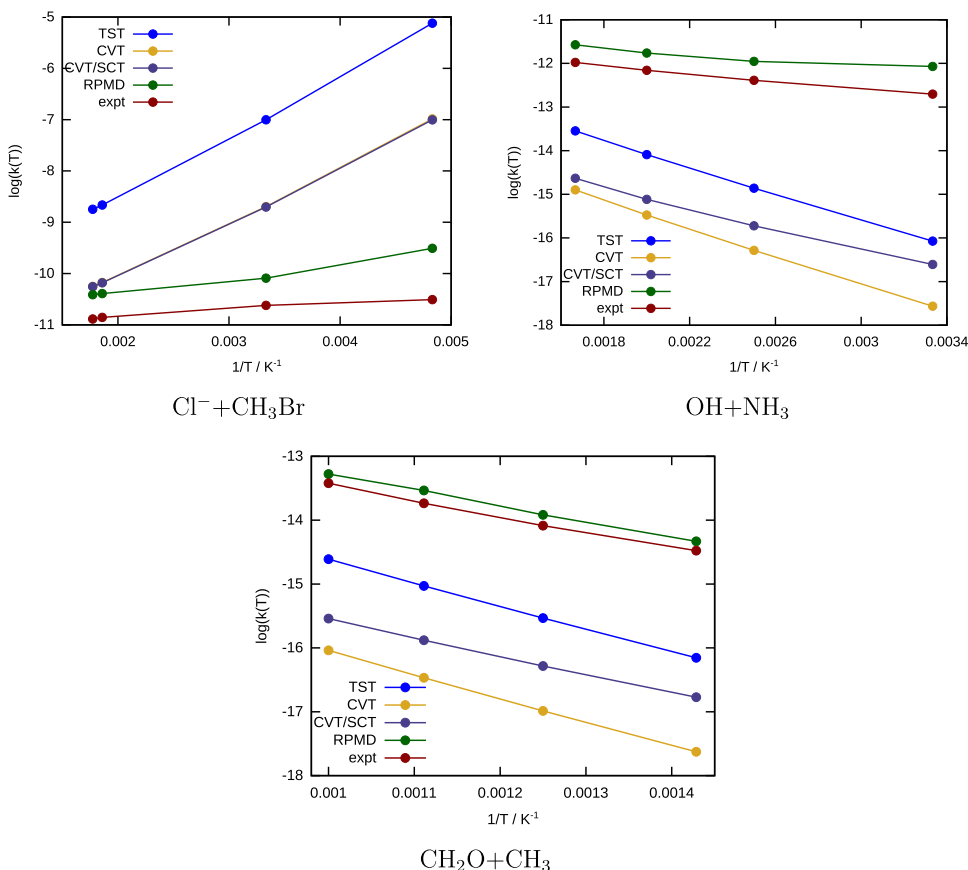


FIG. 5. Temperature-dependent rate constants for the three presented example reactions. The shown TST, CVT, and CVT/SCT rate constants are calculated based on the quantum-chemical reference methods, equivalent to TST_{ref}, CVT, and CVT/SCT_{ref} in Table I.

data is visible. TST_{EQ} and TST_{ref} as well as CVT/SCT_{EQ} and CVT/SCT_{ref} rate constants are within the same order of magnitude.

In summary, it can be said that EVB-QMDFF in combination with RPMDrate was able to reproduce chemical reaction rates of three arbitrarily selected reactions within the same order of magnitude with the reference, in most cases actually within a factor of two or three. This is a strong argument to use EVB-QMDFF as a method for calculating rate constants in chemical practice.

Another important issue is the comparison between TST_{EQ} and TST_{ref} results. Obviously, these numbers are not exactly the same, but—with exception of the slightly worse CVT/SCT values in the $\text{Cl}^- + \text{CH}_3\text{Br}$ reaction—very close to each other, considering that for $k(T)$ values deviations of a factor of 10 are usually taken as good agreement. Hence, these very small deviations show that approximating the DFT- or MP2-data by EVB-QMDFF does not lead to serious distortions of the PES, for the purpose of $k(T)$ calculations.

Summarizing, the results presented in Table I and plotted in Fig. 5 allow one to draw the following three conclusions: (1) We have calculated $k(T)$ with TST and CVT/SCT based directly on the quantum-chemical PES, and with TST and CVT/SCT based on an EVB-QMDFF PES, which in turn has been fitted to the same quantum-chemical data. These two sets of $k(T)$ values agree very well. This tells us that EVB-QMDFF is indeed able to reproduce the quantum-chemical PES very well, at least in the regions that are needed for these calculations, i.e., energies and frequencies of minima, transition state, and the additional PES points in-between. A more direct test for such an agreement would be provided by 1D- and 2D-cuts through these PESs. We did provide such cuts in the supplementary material to Ref. 22, but it is simply not possible to cover a high-dimensional PES in all relevant regions with such cuts. Calculating $k(T)$ is a more indirect method of comparison, but it does include all degrees of freedom. (2) Calculating $k(T)$ data with TST and CVT/SCT directly on the quantum-chemical PES is feasible, but the deviations from experimental $k(T)$ values are well beyond one order of magnitude, indicating problems with the approximations inherent in TST and CVT/SCT or with the quantum-chemical level of theory. (3) Employing the EVB-QMDFF-approximation (as an intermediate level between the quantum-chemistry data and the rate constant calculation) renders a $k(T)$ calculation via RPMD computationally feasible, and the good agreement with experimental $k(T)$ values shows that at least the much larger part of the deviations noted in item (2) is not due to the quantum-chemical method employed but due to TST- and CVT/SCT -approximations.

In spite of these favorable results, two possible error sources still remain in the calculated rate constants.

First, it is possible that MP2/cc-pVTZ or PBE0/def2-QZVPP(-g, -f) is not sufficiently reliable for these reactions. If this is the case, the good results shown here could be due to fortuitous error cancellation. However, this is not very probable because all three reactions that were chosen by chance gave good results, so all three would need to have the same cancellation of errors. Further, other publications in the past,

covering the same or similar reactions, used, e.g., MP2 with similar basis sets at least as the lower level combined with a higher level in the so-called “Dual Level Approach” to calculate TST, CVT, and VTST rate constants, and these compared favorably with experimental results.^{73,74} In another case, MP2 and B3LYP (as another DFT functional) were combined with the “Dual Level Approach” and again gave good agreements with experimental results.⁷⁵ Therefore the present choice of reference method seems to be legitimate for the calculation of at least rate constants in the same order of magnitude with experiment.

The second possible error source is that RPMDrate rate constants, even if they are calculated on an approximately “exact” surface, are systematically wrong or not good enough. This could also lead to a cancellation of errors. One way to eliminate that possibility is to perform wavepacket-dynamics, for example, ML-MCTDH.^{76,77} However, for systems of six or even eight atoms as treated in this publication, this would be too tough and expensive to handle in practice. Fortunately, RPMDrate and wave-packet methods were compared to each other already in the past showing very small deviations between both methods for the $\text{H} + \text{CH}_4$ and the $\text{F} + \text{HCl}$ reactions.^{31,78} This indicates that RPMD is able, at least in the case of small systems with parametrized potential functions, of calculating results which are comparable to wavepacket dynamics.

Finally, we would like to emphasize that the RPMD rates shown above were produced with very conservative program settings, leading to very many PES evaluations. For example, in the $\text{OH} + \text{NH}_3$ reaction, the RPMD calculations at 300 and 400 K took a total of $8 \cdot 10^{10}$ time steps. Very likely, this can be reduced by a few orders of magnitude, without severely compromising the results. But even after such a reduction, doing the same calculation with on-the-fly *ab initio* or DFT dynamics would be a formidable or even impossible task. With EVB-QMDFF as an intermediate layer, such calculations are well within reach on low-end hardware. The above results show that this advantage of EVB-QMDFF does not lead to significant PES distortions, even for the non-trivial task of $k(T)$ calculations, where energy deviations tend to be magnified exponentially.

V. CONCLUSIONS

With the present work, we have shown that reaction rate constants $k(T)$ can be calculated for an expensive PES (e.g., at an *ab initio* or DFT level) with limited expense but very good accuracy. The expense is somewhat higher than for the simplest traditional TST recipe, and very similar to that required for more advanced recipes of the VTST type. The accuracy of the final $k(T)$ data, however, is much better.

The key is the introduction of a system-specific force field (EVB-QMDFF) as an intermediate level. This makes it possible to use advanced methods for $k(T)$ calculation that require huge amounts of PES data, without incurring extreme additional computational costs. At the same time, the loss in accuracy due to this intermediate force field is insignificant, even for the critical task of $k(T)$ evaluation, because the force field is not a universal compromise fit but generated from

scratch for every given elementary reaction step, using the highly versatile but accurate QMDFF functional form. Furthermore, there is zero choice (and hence zero human time investment) in generating the reference data needed for reactant QMDFF and the product QMDFF, and very little choice in generating the EVB coupling of these two. Hence, in contrast to the generation of global, general force fields, this EVB-QMDFF generation step can, and has been, be automatized in a black-box fashion.

This opens the door to automated mass-production of $k(T)$ data, which is needed in many areas, for example, to study vast kinetic networks in combustion chemistry or atmospheric chemistry, or to drive KMC simulations that coarse-grain chemistry towards macroscopic scales of time and matter. In upcoming collaborations, we will use this approach to aid KMC simulations of plasma-surface interactions. This application will not only address larger systems but also a broader range of interactions (from van der Waals via covalent to ionic) and a qualitative change from isolated molecules to extended surfaces.

As side effects, with the present work we have extended EVB-QMDFF to even more flexible EVB couplings by incorporating distributed Gaussians, and we have demonstrated sufficient accuracy of EVB-QMDFF in regions away from the reaction path, in effectively all degrees of freedom.

SUPPLEMENTARY MATERIAL

See [supplementary material](#) for detailed tests on the deviation between EVB-QMDFF and reference data changes with number and types of reference data items, for a full list of RPMD settings including convergence tests, and for potentials of mean force and transmission coefficients, for all three example reactions.

ACKNOWLEDGMENTS

The authors thank Stefan Grimme for providing us with his original QMDFF program and for helpful advice on its use. They also thank the Truhlar group for permission to download and use their POLYRATE program. They further thank Yury Suleimanov for the permission to download and use his RPMDrate program.

¹A. P. J. Jansen, *An Introduction to Monte Carlo Simulations of Surface Reactions*, Lecture Notes on Physics Vol. 856 (Springer, Berlin, Heidelberg, 2012).

²A. Chatterjee and D. G. Vlachos, *J. Comput.-Aided Mater. Des.* **14**, 253–308 (2007).

³M. Stamatakis and D. G. Vlachos, *ACS Catal.* **2**, 2648–2663 (2012).

⁴W. H. Miller, *J. Phys. Chem. A* **102**, 793–806 (1998).

⁵G. Nyman, *Int. J. Quantum Chem.* **114**, 1183–1198 (2014).

⁶U. Manthe, *Mol. Phys.* **109**, 1415–1426 (2011).

⁷J. Meisner and J. Kästner, *Angew. Chem., Int. Ed.* **55**, 5400–5413 (2016).

⁸W. K. den Otter and W. J. Briels, *J. Chem. Phys.* **106**, 5494 (1997).

⁹W. K. den Otter and W. J. Briels, *J. Am. Chem. Soc.* **120**, 13167 (1998).

¹⁰J. B. Anderson, *Adv. Chem. Phys.* **91**, 381 (1995).

¹¹T. Seideman and W. H. Miller, *J. Chem. Phys.* **95**, 1768 (1991).

¹²T. Seideman and W. H. Miller, *J. Chem. Phys.* **96**, 4412 (1992).

¹³T. Seideman and W. H. Miller, *J. Chem. Phys.* **97**, 2499 (1992).

¹⁴U. Manthe and W. H. Miller, *J. Chem. Phys.* **99**, 3411 (1993).

¹⁵U. Manthe, T. Seideman, and W. H. Miller, *J. Chem. Phys.* **101**, 4759 (1994).

¹⁶D. H. Zhang and J. C. Light, *J. Chem. Phys.* **104**, 6184 (1996).

- ¹⁷D. G. Truhlar, B. C. Garrett, and S. J. Klippenstein, *J. Phys. Chem.* **100**, 12771 (1996).
- ¹⁸L.-P. Ju, K.-L. Han, and J. Z. H. Zhang, *J. Comput. Chem.* **30**, 305 (2009).
- ¹⁹D. G. Truhlar and B. C. Garrett, *Acc. Chem. Res.* **13**, 440 (1980).
- ²⁰T. V. Albu, J. C. Corchado, and D. G. Truhlar, *J. Phys. Chem. A* **105**, 8465–8487 (2001).
- ²¹S. Grimme, *J. Chem. Theory Comput.* **10**, 4497–4514 (2014).
- ²²B. Hartke and S. Grimme, *Phys. Chem. Chem. Phys.* **17**, 16715–16718 (2015).
- ²³I. R. Craig and D. E. Manolopoulos, *J. Chem. Phys.* **121**, 3368 (2004).
- ²⁴I. R. Craig and D. E. Manolopoulos, *J. Chem. Phys.* **122**, 084106 (2005).
- ²⁵I. R. Craig and D. E. Manolopoulos, *J. Chem. Phys.* **123**, 034102 (2005).
- ²⁶R. Colleparo-Guevara, Y. V. Suleimanov, and D. E. Manolopoulos, *J. Chem. Phys.* **130**, 174713 (2009).
- ²⁷S. Habershon, D. E. Manolopoulos, T. E. Markland, and T. F. Miller III, *Annu. Rev. Phys. Chem.* **64**, 387–413 (2013).
- ²⁸J. O. Richardson and S. C. Althorpe, *J. Chem. Phys.* **131**, 214106 (2009).
- ²⁹T. J. H. Hele and S. C. Althorpe, *J. Chem. Phys.* **144**, 174107 (2016).
- ³⁰Y. V. Suleimanov, F. J. Aoiz, and H. Guo, *J. Phys. Chem. A* **120**, 8488 (2016).
- ³¹M. Bai, D. Lu, Y. Li, and J. Li, *Phys. Chem. Chem. Phys.* **18**, 32031–32041 (2016).
- ³²A. V. Marenich, S. V. Jerome, C. J. Cramer, and D. G. Truhlar, *J. Chem. Theory Comput.* **8**, 527–541 (2012).
- ³³K. B. Wiberg, *Tetrahedron* **24**, 1083–1096 (1968).
- ³⁴I. Mayer, *Chem. Phys. Lett.* **97**, 270–274 (1983).
- ³⁵K. Farah, F. Müller-Plathe, and M. C. Bhm, *Chem. Phys. Chem.* **13**, 1127 (2012).
- ³⁶A. Warshel, *J. Am. Chem. Soc.* **102**, 6218 (1980).
- ³⁷F. Jensen and P.-O. Norrby, *Theor. Chem. Acc.* **109**, 1 (2003).
- ³⁸D. E. Sagnella and M. E. Tuckerman, *J. Chem. Phys.* **108**, 2073–2083 (1998).
- ³⁹D. R. Glowacki, A. J. Orr-Ewing, and J. N. Harvey, *J. Chem. Phys.* **134**, 214508 (2011).
- ⁴⁰V. B. Luzhkov, *Chem. Phys. Lett.* **345**, 345–352 (2001).
- ⁴¹K. Levenberg, *Q. Appl. Math.* **2**, 164–168 (1944).
- ⁴²D. W. Marquardt, *J. Soc. Ind. Appl. Math.* **11**, 431–441 (1963).
- ⁴³C. Minichino and G. A. Voth, *J. Phys. Chem. B* **101**, 4544–4552 (1996).
- ⁴⁴Y.-T. Chang and W. H. Miller, *J. Phys. Chem.* **94**, 5884–5888 (1990).
- ⁴⁵Y.-T. Chang, C. Minichino, and W. H. Miller, *J. Chem. Phys.* **96**, 4341–4355 (1992).
- ⁴⁶H. B. Schlegel and J. L. Sonnenberg, *J. Chem. Theory Comput.* **2**, 905–911 (2006).
- ⁴⁷J. L. Sonnenberg, K. F. Wong, G. A. Voth, and H. B. Schlegel, *J. Chem. Theory Comput.* **5**, 949–961 (2009).
- ⁴⁸K. F. Wong, J. L. Sonnenberg, F. Paesani, T. Yamamoto, J. Vanicek, W. Zhang, H. B. Schlegel, D. A. Case, T. E. Cheatham III, W. H. Miller, and G. A. Voth, *J. Chem. Theory Comput.* **6**, 2566–2580 (2010).
- ⁴⁹Y. Kim, J. C. Corchado, J. Villa, J. Xing, and D. G. Truhlar, *J. Chem. Phys.* **112**, 2718–2735 (2000).
- ⁵⁰O. Tishchenko and D. G. Truhlar, *J. Chem. Phys.* **132**, 084109 (2010).
- ⁵¹J. K. Sonnenberg and H. B. Schlegel, The Empirical Valence Bond Toolkit for Mathematica, <http://chem.wayne.edu/schlegel/>.
- ⁵²D. A. Case, R. M. Betz, W. Botello-Smith, D. S. Cerutti, T. E. Cheatham III, T. A. Darden, R. E. Duke, T. J. Giese, H. Gohlke, A. W. Goetz, N. Homeyer, S. Izadi, P. Janowski, J. Kaus, A. Kovalenko, T. S. Lee, S. LeGrand, P. Li, C. Lin, T. Luchko, R. Luo, B. Made, D. Mermelstein, K. M. Merz, G. Monard, H. Nguyen, H. T. Nguyen, I. Omelyan, A. Onufriev, D. R. Roe, A. Roitberg, C. Sagui, C. L. Simmerling, J. Swails, R. C. Walker, J. Wang, R. M. Wolf, X. Wu, L. Xiao, D. M. York, and P. A. Kollman, AMBER, 2016.
- ⁵³P. Pulay and G. Fogarasi, *J. Chem. Phys.* **96**, 2856–2860 (1992).
- ⁵⁴Y. V. Suleimanov, J. W. Allen, and W. H. Green, *Comput. Phys. Commun.* **184**, 833–840 (2013).
- ⁵⁵Y. V. Suleimanov, R. Colleparo-Guevara, and D. E. Manolopoulos, *J. Chem. Phys.* **134**, 044131 (2011).
- ⁵⁶M. J. Frisch, G. W. Trucks, H. B. Schlegel, G. W. Scuseria, M. A. Robb, J. R. Cheeseman, G. Scalmani, V. Barone, B. Mennucci, G. A. Petersson, H. Nakatsuji, M. Caricato, X. Li, H. P. Hratchian, A. F. Izmaylov, J. Bloino, G. Zheng, J. L. Sonnenberg, M. Hada, M. Ehara, K. Toyota, R. Fukuda, J. Hasegawa, M. Ishida, T. Nakajima, Y. Honda, O. Kitao, H. Nakai, T. Vreven, J. A. Montgomery, Jr., J. E. Peralta, F. Ogliaro, M. Bearpark, J. J. Heyd, E. Brothers, K. N. Kudin, V. N. Staroverov, R. Kobayashi, J. Normand, K. Raghavachari, A. Rendell, J. C. Burant, S. S. Iyengar, J. Tomasi, M. Cossi, N. Rega, J. M. Millam, M. Klene, J. E. Knox,

- J. B. Cross, V. Bakken, C. Adamo, J. Jaramillo, R. Gomperts, R. E. Stratmann, O. Yazyev, A. J. Austin, R. Cammi, C. Pomelli, J. W. Ochterski, R. L. Martin, K. Morokuma, V. G. Zakrzewski, G. A. Voth, P. Salvador, J. J. Dannenberg, S. Dapprich, A. D. Daniels, O. Farkas, J. B. Foresman, J. V. Ortiz, J. Cioslowski, D. J. Fox, *GAUSSIAN 09*, Revision D.01, Gaussian, Inc., Wallingford, CT, 2009.
- ⁵⁷F. Neese, *Wiley Interdiscip. Rev.: Comput. Mol. Sci.* **2**, 73–78 (2012).
- ⁵⁸K. Fukui, *Acc. Chem. Res.* **14**, 363–368 (1981).
- ⁵⁹C. Adamo and V. Barone, *J. Chem. Phys.* **110**, 6158–6170 (1999).
- ⁶⁰S. Grimme, *Wiley Interdiscip. Rev.: Comput. Mol. Sci.* **1**, 211–228 (2011).
- ⁶¹F. Weigend and R. Ahlrichs, *Phys. Chem. Chem. Phys.* **7**, 3297–3305 (2007).
- ⁶²F. Weigend, *Phys. Chem. Chem. Phys.* **8**, 1057–1065 (2006).
- ⁶³T. H. Dunning, Jr., *J. Chem. Phys.* **90**, 1007–1023 (1989).
- ⁶⁴S. Thallmair, M. K. Roos, and R. de Vivie-Riedle, *J. Chem. Phys.* **144**, 234104 (2016).
- ⁶⁵J. P. P. Zauleck, S. Thallmair, M. Loipersberger, and R. de Vivie-Riedle, *J. Chem. Theory Comput.* **12**, 5698 (2016).
- ⁶⁶J. Zheng, S. Zhang, B. J. Lynch, J. C. Corchado, Y.-Y. Chuang, P. L. Fast, W.-P. Hu, Y.-P. Liu, G. C. Lynch, K. A. Nguyen, C. F. Jackels, A. Fernandez Ramos, B. A. Ellingson, V. S. Melissas, J. Villà, I. Rossi, E. L. Coitiño, J. Pu, T. V. Albu, R. Steckler, B. C. Garrett, A. D. Isaacson, and D. G. Truhlar, POLYRATE-version 2010, University of Minnesota, Minneapolis, 2010.
- ⁶⁷Y. Li, Y. V. Suleimanov, J. Li, W. H. Green, and H. Guo, *J. Chem. Phys.* **138**, 094307 (2013).
- ⁶⁸E. Gonzalez-Lavado, J. C. Corchado, Y. V. Suleimanov, W. H. Green, and J. Espinosa-Garcia, *J. Phys. Chem. A* **118**, 3243–3252 (2014).
- ⁶⁹J. Zuo, Y. Li, H. Guo, and D. Xie, *J. Phys. Chem. A* **120**, 3433–3440 (2016).
- ⁷⁰A. A. Viggiano, J. S. Paschkewitz, R. A. Morris, J. F. Paulson, A. Gonzalez-Lafont, and D. G. Truhlar, *J. Am. Chem. Soc.* **113**, 9404–9405 (1991).
- ⁷¹J. B. Jeffries and G. P. Smith, *J. Phys. Chem.* **90**, 487–491 (1986).
- ⁷²W. B. DeMore, *J. Phys. Chem.* **100**, 5813–5820 (1996).
- ⁷³J. C. Corchado, J. Espinosa-Garcia, W.-P. Hu, I. Rossi, and D. G. Truhlar, *J. Phys. Chem.* **99**, 687–694 (1995).
- ⁷⁴Z.-F. Xu and C.-C. Sun, *J. Mol. Struct.: THEOCHEM* **459**, 37–46 (1999).
- ⁷⁵S. Lobachevsky, C. H. Schiesser, C. Y. Lin, and M. L. Coote, *J. Phys. Chem. A* **112**, 13622–13627 (2008).
- ⁷⁶M. Beck, A. Jäckle, G. Worth, and H.-D. Meyer, *Phys. Rep.* **324**, 1–105 (2000).
- ⁷⁷H. Wang and M. Thoss, *J. Chem. Phys.* **119**, 1289–1299 (2003).
- ⁷⁸Q. Meng, J. Chen, and D. H. Zhang, *J. Chem. Phys.* **143**, 101102 (2015).